

Modeling and Implementation of the Direct Torque Control Technique Used in a Relevant PV-powered Pumping Application

Sebastien Jacques, Zahra Mokrani, Said Aissou, Djamila Rekioua, Toufik Rekioua

▶ **To cite this version:**

Sebastien Jacques, Zahra Mokrani, Said Aissou, Djamila Rekioua, Toufik Rekioua. Modeling and Implementation of the Direct Torque Control Technique Used in a Relevant PV-powered Pumping Application. Journal of Electrical Engineering (JEE), 2018. hal-02296862

HAL Id: hal-02296862

https://univ-tours.hal.science/hal-02296862

Submitted on 25 Sep 2019

HAL is a multi-disciplinary open access archive for the deposit and dissemination of scientific research documents, whether they are published or not. The documents may come from teaching and research institutions in France or abroad, or from public or private research centers.

L'archive ouverte pluridisciplinaire **HAL**, est destinée au dépôt et à la diffusion de documents scientifiques de niveau recherche, publiés ou non, émanant des établissements d'enseignement et de recherche français ou étrangers, des laboratoires publics ou privés.

Modeling and Implementation of the Direct Torque Control Technique Used in a Relevant PV-powered Pumping Application

Sébastien JACQUES
University of Tours, GREMAN CNRS UMR 7347 INSA CVL, Tours, France
7 avenue Marcel Dassault, 37200 Tours, France, Phone: +33 7 604 071 42, Email: sebastien.jacques@univ-tours.fr

Zahra MOKRANI Said AISSOU Djamila REKIOUA Toufik REKIOUA
Electrical Engineering Department, University of Bejaia, Algeria
Bejaia, 0600, Algeria

Abstract: *The main purpose of this paper is to model and implement the direct torque control technique for driving a single phase induction motor in a low-cost and easily transportable photovoltaic-powered pumping system. To achieve this goal, a comparative investigation of the performance characteristics of different control techniques, such as closed loop scalar control (voltage/frequency) and indirect field oriented control Technique, is presented. From this study and according to complexity, robustness, difficulty of implementation and cost, an accurate and simple photovoltaic water pumping sys-tem is developed. This system is based on a single-phase motor supplied by a three-phase inverter using the direct torque control method. This standalone photovoltaic system is dedicated to water pumping, especially in rural areas that have no access to national grid but have sufficient amount of solar radiation. Simulation modeling (Matlab / Simulink) and experimental test results are presented to demonstrate the effectiveness and relevance of the proposed system designed for industrial use.*

Key words: *Direct torque control (DTC), single phase induction motor (SPIM), low cost and transportable photovoltaic pumping system.*

1. Introduction

For many years now, electric motors have been commonly used in a wide range of industrial applications such as fans, pumps, machine tools, household appliances or, in an original way, implantable medical devices [1,2]. Whatever the type of motor (direct current or DC, alternating current or AC), there are two key elements. The first one is composed of an armature (a conductive coil) surrounded by a field magnet responsible for creating an electromotive force that causes the shaft to rotate, generating mechanical torque. The second one is a commutator composed of a set of contacts attached to the armature shaft. Its role is to keep reversing the direction of current flow in the armature as it turns, thus ensuring that the motor continues to turn.

Even if DC motors have a very long history, including the fact that they offer the easiest way to control the flux and torque in any application requiring drives with variable speed and position, harsh applications (in particular, dry and warm environments) can greatly affect their lifetime [3]. For example, regarding brush DC motors, these conditions may increase the wear-out of the brushes and accelerate the breakdown of the commutator and bearings. The use of brushless DC (BLDC) motors makes it possible to partly overcome these difficulties. However, BLDC motors need sophisticated electronic control circuitry as well as some way to continuously determine the position of the rotor [4].

AC electric motors and particularly induction motors (IM) have obtained special interests from the industry since their invention. Indeed, these motors do not require mechanical commutation, separate-excitation or self-excitation for all or part of the energy transferred from stator to rotor, as for instance in DC motors. IM are currently used in variable-frequency drive (VFD) applications such as in variable-torque centrifugal fan, pump or compressor load applications [5].

Despite some disadvantages such as high starting current and speed control that may uneasy to drive, the reasons for this success are amongst others: higher reliability due to the absence of brushes, higher robustness, easiness to build, inexpensive, and higher efficiency (about 80%). However, the use of an induction motor in any application is challenging, because of its complex mathematical model, its non-linear behavior during saturation mode and the electrical parameters' oscillation which is particularly temperature-dependent. As a consequence, the control of an induction motor is still a major issue [6].

In recent years, application of advanced control techniques has increased significantly for induction motor drive systems owing to the technological improvements, especially in power electronics and microprocessor technologies.

The scalar control, also called V/f control, well-known for its simplicity, was the first command introduced in the industry. This technique consists in monitoring the induction motor speed by adjusting the magnitude of stator voltages and frequency in such a way that the air gap flux is always maintained at the desired value in steady-state.

Nevertheless, using this technique, field orientation of the motor is not used. Indeed, the frequency and the voltage are the main control variables and are applied

to the stator windings. The status of the rotor is ignored, meaning that no speed or position signal is fed back. Therefore, torque can-not be controlled with any degree of accuracy.

The field oriented control (FOC), which is one of the vector control methods, is currently a particularly interesting research area [7]. This technique consists in separately controlling the torque producing and magnetizing flux components. Thus, the stator currents are represented by a vector. In a sense, the aim is to imitate DC motors' operation by transforming a three phase time and speed de-pendent system into a two coordinate time invariant sys-tem. The implementation of FOC may be complex because it requires current regulator, coordinate transformation, generator of pulse width modulation (PWM) signals and timers.

Direct torque control (DTC) has been developed to re-place traditional PWM drives of the open- and closed-loop type used in FOC [8]. This method describes the way in which the control of torque and speed are directly based on the electromagnetic state of the motor in comparison with PWM drives which use input frequency and voltage. There are many benefits of the DTC technique: torque response, accurate torque control at low frequencies, torque repeatability, motor static and dynamic speed accuracy.

The ultimate challenge of this paper is to model and implement the DTC technique to control a 370 W induction motor used in a low-cost and easily transportable photo-voltaic-powered pumping system (35 l/min).

First of all, the present manuscript describes the application requirements and the reasons related to the implementation of the DTC method to control the induction motor. Then, a comprehensive overview of control techniques for electrical machines is proposed. The aim is to justify the choice of the DTC method. The fourth section of this paper is dedicated to the DTC technique modeling and its relevance through experimental measurements. Finally, a discussion is proposed to compare the model outputs and test results.

2. Review of the Background and Motivations

Water pumping is one of the most significant photovoltaic (PV) applications, especially to overcome the need for water in mountainous or remote locations and improve isolated populations' life. Moreover it reduces the negative impact of diesel installations on the environment. For example, on average, for an operating time of 5 hours per day, 1,000 PV-pumps, each with a nominal power equal to 950 W, can support the reduction of CO2 emissions by 4.2 tons a year. This positive outcome shows the interest of such a PV system in industrial applications, such as water pumping [9].

Although the single phase induction motor (SPIM) is not widely accepted in literature, it can be an excellent choice due to consideration of cost, availability, simplicity of control and operation. Regarding irrigation and pumping water applications, the water flow regulation is needed. The control techniques applied to induction machine allow this regulation and offer the best performances [10,11].

Figure 1 shows the general architecture of a PV pumping system.

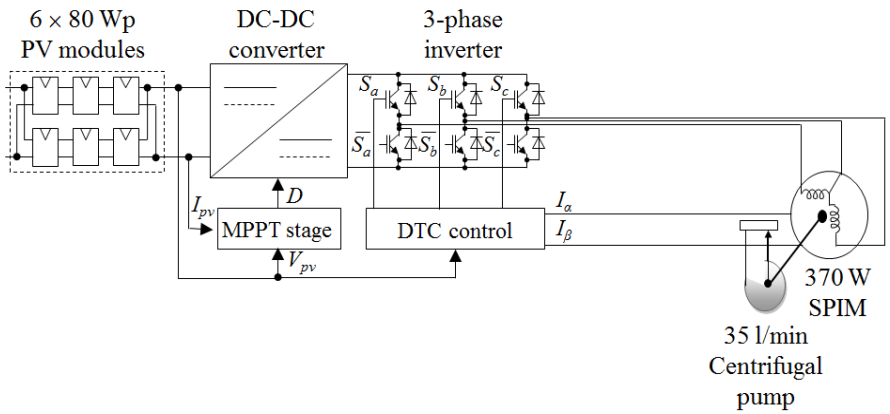


Fig. 1. General architecture of the photovoltaic-powered pumping application.

It is composed of six 80 Wp PV modules, a DC-DC converter (boost converter) controlled by a maximum power point tracking (MPPT) system, 3-phase inverter and 370 W single-phase motor pump. It is important to note that this kind of motor is easily transportable thanks to its very compact size (length, width and height equal to 135 mm, 245 mm and 176 mm, respectively) and low gross weight (less than 10 kg). The starting capacitance was suppressed to control the SPIM, and particularly to have access to the connection point between the two windings. This operation permits to supply the SPIM by a three-phase inverter that gives the phase shift to the motor. The first one is composed of an armature (a conductive coil) surrounded by a field magnet responsible for creating an electromotive force that causes the shaft to rotate,

generating mechanical torque. The second one is a commutator composed of a set of contacts attached to the armature shaft. Its role is to keep reversing the direction of current flow in the armature as it turns, thus ensuring that the motor continues to turn.

2.1. Modeling of the PV Generator

The one-diode mathematical model of the solar cell is given by Equation (1) and Equation (2), where: I_{pv} is the output-terminal current, I_{ph} is the light-generated current, I_d is the diode-current, I_{sh} is the shunt-leakage current, I_0 is the saturation current of the diode, q is the electron charge, V_{pv} is the output-terminal voltage, R_s is the serial resistance, A is an ideality factor of the *pn* junction, k is the Boltzmann's constant, T_j is the junction temperature of the solar cell, and R_{sh} is the shunt resistance [12-14].

$$I_{pv} = I_{ph} - I_d - I_{sh} \quad (1)$$

$$I_{pv} = I_{ph} - I_0 \cdot \left[\exp\left(\frac{q.(V_{pv} + R_s.I_{pv})}{A\,k\,.T_j} \right) - 1 \right] - \frac{V_{pv} + R_s.I_{pv}}{R_{sh}} \quad (2)$$

Table 1 summarizes the parameters of the PV module (SUNTECH STP080S-12/Bb) used in this application.

A DC-DC boost converter is used to track the MPPT in order to boost the DC voltage of the PV module. The duty cycle (D) of the switch is obtained using the MPPT controller based on the Perturb & Observe (P&O) technique. The output voltage (V_{out}) and output current (I_{out}) of the converter are given by Equation (3) and Equation (4) [15,16].

$$V_{out} = V_{pv}\left(\frac{1}{1-D} \right) \quad (3)$$

$$I_{out} = I_{pv}(1-D) \quad (4)$$

Table 1
Main features of the SUNTECH STP080S-12/Bb PV module (36 monocrystalline silicon solar cells)

Symbol	Parameter	Value
P_{pv}	Peak power	80 Wp
I_{mpp}	Maximum current at MPP	4.58 A
V_{mpp}	Maximum voltage at MPP	17.5 V
I_{SC}	Short-circuit current	4.95 A
V_{OC}	Open-circuit voltage	21.9 V
NOCT	Nominal Operating Cell Temperature	48 °C ± 2 °C
α_{SC}	Short-circuit current temperature coefficient	0.020%/K
β_{OC}	Open-circuit voltage temperature coefficient	-0.34%/K

2.2. Modeling of the Three-Phase Inverter

The function of the inverter is to convert the direct voltage into alternating one. Figure 2 shows the general architecture of the inverter. The DC-AC converter is composed of 6 insulated gate bipolar transistors (IGBTs) to control the 3-phase motor.

The aim of this kind of system is to manage the amplitude and frequency of the stator voltages. The three-phase inverter model contains eight switching states. Figure 3 shows the representation of each IGBT state based on a vector presentation.

The stator phase voltages are described in Equation (5) using literature [17,18], where $V_{(a,b,c)}$ are the three phase stator voltages, V_{dc} is the DC link voltage and $S_{(a,b,c)}$ are the switching functions that can take 2 logic values: 0 or 1.

The output voltage of the inverter is defined in Equation (6) and Equation (7) using the vector presentation.

The three-phase voltage system is given by Equation (8).

Then, v can be expressed using Equation (9). This equation allows the determination of the voltage for each sector using the vector presentation.

The inverter is controlled by the DTC technique which is detailed in the next section.

$$\begin{bmatrix} V_{an} \\ V_{bn} \\ V_{cn} \end{bmatrix} = \frac{V_{dc}}{3} \begin{bmatrix} 2 & -1 & -1 \\ -1 & 2 & -1 \\ -1 & -1 & 2 \end{bmatrix} \cdot \begin{bmatrix} S_a \\ S_b \\ S_c \end{bmatrix} \quad (5)$$

$$\vec{v} = v_\alpha + j v_\beta \quad (6)$$

$$\begin{bmatrix} v_\alpha \\ v_\beta \end{bmatrix} = \frac{2}{3} \begin{bmatrix} 1 & -\frac{1}{2} & -\frac{1}{2} \\ 0 & \frac{\sqrt{3}}{2} & -\frac{\sqrt{3}}{2} \end{bmatrix} \begin{bmatrix} V_{an} \\ V_{bn} \\ V_{cn} \end{bmatrix} \quad (7)$$

$$\begin{bmatrix} V_{an} \\ V_{bn} \\ V_{cn} \end{bmatrix} = V_m \begin{bmatrix} \cos(\omega t + \varphi) \\ \cos(\omega t + \varphi - \frac{2\pi}{3}) \\ \cos(\omega t + \varphi - \frac{4\pi}{3}) \end{bmatrix} \quad (8)$$

$$v = \frac{2}{3} V_{dc} \left(S_a + S_b e^{j\left(\frac{2}{3}\right)\pi} + S_c e^{j\left(\frac{4}{3}\right)\pi} \right) \quad (9)$$

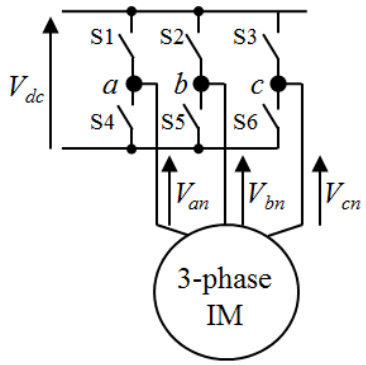


Fig. 2. General architecture of the photovoltaic-powered pumping application.

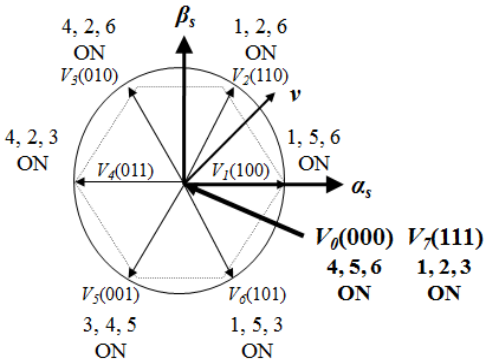


Fig. 3. Operating conditions of 3-phase inverter: vector presentation of the voltages.

2.3. Modeling of the SPIM

The single-phase induction machine (SPIM) is selected for this type of application for its low cost, high robustness and high reliability. The structure of this kind of motor is very simple. It is composed of two windings: the main one and the auxiliary one. Its operation requires a shift capacitance. So, the main and auxiliary windings are phase shifted by 90 degrees. As a consequence, this motor acts as 2-phase motor [10], [19,20]. The DC-AC converter is composed of 6 insulated gate bipolar transistors (IGBTs) to control the 3-phase motor.

The SPIM is a nonlinear and unsymmetrical system. It is quite difficult to model the motor operation using equations because of the different stator resistances. As reported in literature, the stator and rotor voltage equations can be represented in a stationary reference frame using Equation (10) and Equation (11) [10,11], [20-22].

Equation (12) and Equation (13) give the stator flux and electromagnetic torque equations. The parameters of these equations are defined below:

- $V_{s\alpha}$, $V_{s\beta}$: α-β stator voltages.
- $i_{s\alpha}$, $i_{s\beta}$, $i_{r\alpha}$, $i_{r\beta}$: α-β stator and rotor currents.
- $\Phi_{s\alpha}$, $\Phi_{s\beta}$, $\Phi_{r\alpha}$, $\Phi_{r\beta}$: α-β stator and rotor flux.
- Γ_e: electromagnetic torque.
- $R_{s\alpha}$, $R_{s\beta}$, R_r: α-β stator resistances, rotor resistance.
- L_s, L_r: stator and rotor inductances.
- M: mutual inductance.
- P: machine pole pairs.

$$\begin{cases} V_{s\alpha} = R_{s\alpha} i_{s\alpha} + \dfrac{d\Phi_{s\alpha}}{dt} \\ V_{s\beta} = R_{s\beta} i_{s\beta} + \dfrac{d\Phi_{s\beta}}{dt} \end{cases} \quad (10)$$

$$\begin{cases} 0 = R_r i_{r\alpha} + \dfrac{d\Phi_{r\alpha}}{dt} + \omega\, \Phi_{r\beta} \\ 0 = R_r i_{r\beta} + \dfrac{d\Phi_{r\beta}}{dt} - \omega\, \Phi_{r\alpha} \end{cases} \quad (11)$$

$$\begin{cases} \Phi_{s\alpha} = L_s i_{s\alpha} + M i_{r\beta} \\ \Phi_{s\beta} = M i_{s\beta} + L_r i_{s\beta} \end{cases} \quad (12)$$

$$\Gamma_e = \frac{3P}{2}\frac{M}{Lr}(\Phi_{r\beta} i_{s\alpha} - \Phi_{r\alpha} i_{s\beta}) \quad (13)$$

2.4. Modeling of the Centrifugal Pump

As shown in Equation (14), the centrifugal pump load torque (T_r) is proportional to the square of the rotor speed (Ω). In this equation, k_c is a proportionality constant [15-16].

Equation (15) gives the H-Q characteristic of the pipe network, where H, Q, H_g, Ψ are the total head, the flow rate, geodetic head and the constant depending on conduit diameter on all frictional losses of the pipe network, respectively [23-24].

$$T_r = k_c.\Omega^2 \quad (14)$$

$$H = H_g + \Psi Q^2 \quad (15)$$

3. Comprehensive Overview of Control Methods for Electrical Machines

Many techniques of variable speed control are well-described in literature, such as scalar control using opened or closed loop, vector control that involves direct and indirect field oriented control, and direct torque control.

In this section of the paper, the advantages and draw-backs of the closed loop scalar control, indirect field oriented control (IFOC) and direct torque control (DTC) techniques are discussed. In particular, their interest in the control of induction motor is highlighted.

3.1. Closed Loop Scalar Control

Figure 4 shows the scalar control method using a closed loop speed. Its principle that is based on Equation (16) consists in varying the magnitude of the stator voltage (V_s) and stator frequency (f), while maintaining the V_s / f–parameter constant [25-29]. In this equation, R_s and I_s are the stator resistance and stator current, respectively. As described in Figure 4, the speed sensor is very helpful to calculate the rotation speed (ω_m) of the motor. The value of this parameter is compared to the reference speed (ω_m*). The error is introduced to the proportional – integral (PI) controller

to get the slip command (ω_r). This slip control is added to the speed measured to determine the stator frequency command (ω_s). This one allows obtaining the stator voltage and stator angle (θ_r) using the V / f function generator. The inverter is controlled by a pulse width modulation (PWM) system.

Ignoring the voltage drop across the stator resistance, the stator flux is given by Equation (17), where λ is constant [25].

In scalar control, flux and torque are linked with frequency and voltage. Moreover, at low voltage, the stator resistance cannot be neglected [6].

As can be seen in Figure 5, even if this control technique is widely used due to its simplicity and low cost, it presents a low accuracy, a small voltage range band and a poor torque response.

$$\Phi_S = \int (V_s - R_s I_s) dt \tag{16}$$

$$\Phi_S = \frac{V_s}{f} = \lambda \tag{17}$$

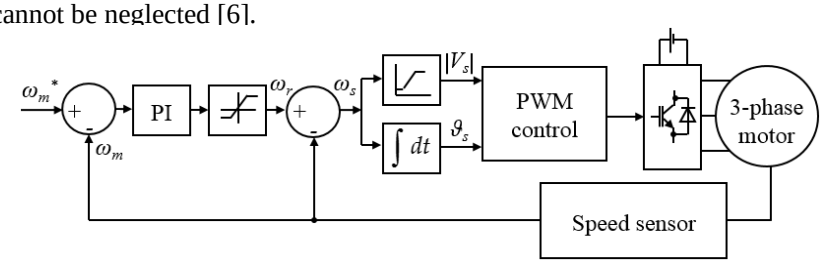


Fig. 4. General schematic of the closed loop scalar control configuration.

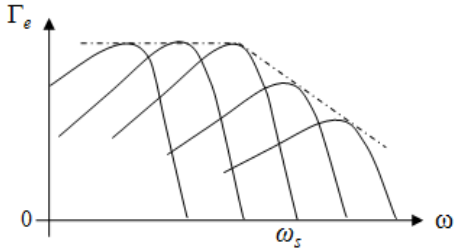


Fig. 5. Torque-speed curve.

3.2. Indirect Field Oriented Control Technique

The vector control technique not only enables to control the amplitude but the phase of the voltage, current and flux in a vector presentation. Its operating principle consists in controlling the flux and torque of an induction machine, separately. Decomposing the stator currents into two components in the (d,q) axes stator reference frame, it is possible to get a behavior similar to that of the DC machine. i_{ds} (resp. i_{qs}) operates on the rotor flux reference Φ_r* (resp. the torque reference Γ_e*), as shown in Equation (18) (where the p-parameter represents the Laplace operator) and Equation (19) [6], [22], [26].

$$\Phi_r^* = \frac{M}{1 + p\frac{L_r}{R_r}} i_{ds}^* \tag{18}$$

$$\Gamma_e^* = P \frac{3}{2} \frac{M}{L_r} \Phi_r^* i_{qs}^* \tag{19}$$

The block diagram of the IFOC technique is presented in Figure 6.

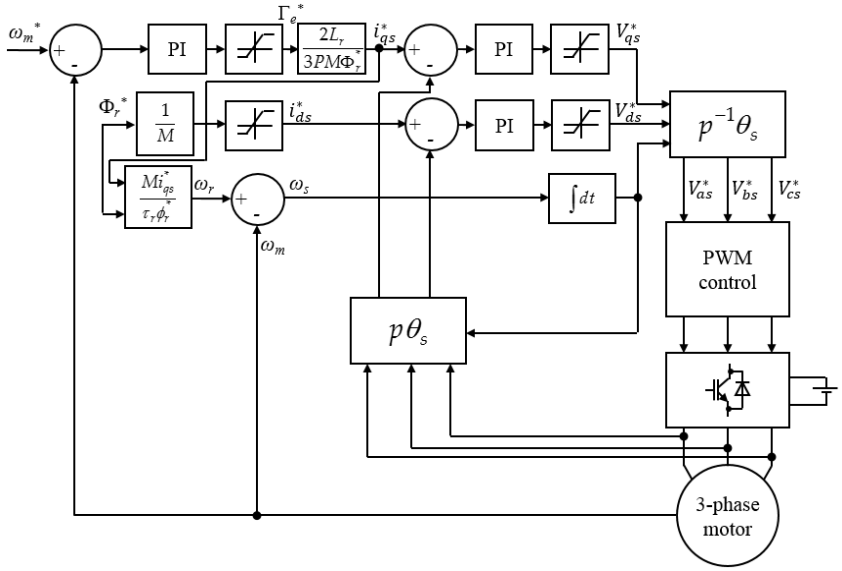


Fig. 6. General implementation of the indirect field oriented control method used to drive 3-phase induction motor.

The torque reference (Γ_e*) is obtained by the regulation of the speed reference (ω_m*) to extract the stator current components (i_{qs}*, i_{ds}*) with the regulation of the rotor flux reference (Φ_r*) too. Using the PI regulator, the obtained currents enables to get the stator voltage references (V_{qs}*, V_{ds}*). To extract the synchronous angular velocity, a speed sensor is used to estimate the speed of the machine which is added to the slip control (obtained using the Φ_r* and i_{ds}*– parameters).

However, its main drawbacks are the need to warrant high calculation capacity, the use of a PI controller, the need of a speed or position sensor and the precise knowledge of the machine's parameters [27,28].

3.3. Direct Torque Control Technique

Comparing to the IFOC control technique, the DTC method is simple to implement. It depends on the stator resistance parameter and does not use any mechanical sensor [6], [29].

Figure 7 shows the block diagram of the command. The DTC technique is based on the direct control of the stator flux and electromagnetic torque. For this purpose, the selection of the optimal space vector using a hysteresis controller is required. Similarly, the stator flux, electromagnetic torque developed by the machine and its position in terms of flux can be estimated [15].

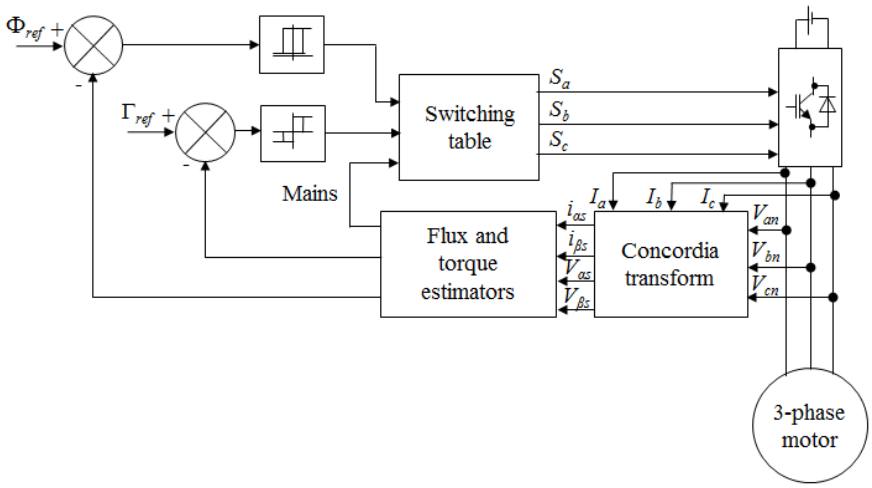


Fig. 7. General implementation of the direct torque control technique used to drive 3-phase induction motor.

As can be seen in Equation (20), the $\Phi_{s\alpha}$ and $\Phi_{s\beta}$– parameters of the stator flux along the (α, β) stator axes are reported in literature [13], [21], [30-32].The stator flux is estimated from Equation (21). The electromagnetic torque is calculated using Equation (22).

The estimated flux and torque are compared to their reference values and the obtained error is used as an input of two (resp. three) levels hysteresis regulators (the first one for the flux and the second one for the torque). The regulator maintains torque and flux errors inside the hysteresis bands as shown in Figure 8 [28].

$$\begin{cases} \Phi_{s\alpha}(t) = \int_0^t (V_{s\alpha} - R_s \times i_{s\alpha})dt \\ \Phi_{s\beta}(t) = \int_0^t (V_{s\beta} - R_s \times i_{s\beta})dt \end{cases} \quad (20)$$

$$\Phi_s = \sqrt{\Phi_{s\alpha}^2 + \Phi_{s\beta}^2} \quad (21)$$

$$\Gamma_e = \frac{3P}{2}\left(\Phi_{s\beta} i_{s\alpha} - \Phi_{s\alpha} i_{s\beta}\right) \quad (22)$$

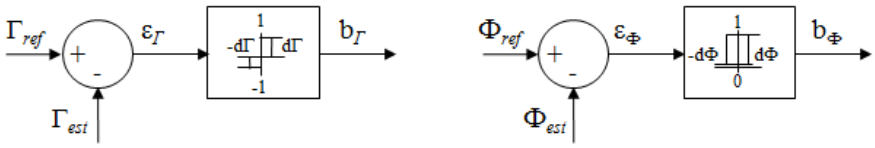


Fig. 8. General outline schematic of 3-level hysteresis regulator.

As proposed in [27], the flux is divided in six equal sectors. Each sector has selected vectors to increase or de-crease the stator flux and torque. To sum up the main facts, if the stator flux vector is in sector named *i* and the motor turns counter clockwise, then:

- If V_{i+1} is selected, Φ_s will increase and Γ_e will increase.
- If V_{i-1} is selected, Φ_s will increase and Γ_e will

decrease.
• If V_{i+2} is selected, Φ_s will decrease and Γ_e will increase.
• If V_{i-2} is selected, Φ_s will decrease and Γ_e will decrease.

For instance, if V_0 or V_7 is selected, then Φ_s will be constant and Γ_e will increase.
The space vector applied in each condition is described in Table 2 [13], [21], [28].
Table 3 sums up the main characteristics of each control technique. This table is necessary to justify the selection of the DTC method. The analysis focuses on the easiest technique to elaborate, the less dependent on machine settings and its cost-effectiveness by avoiding the use of any position sensor.

Table 2
Switching table for the DTC technique

	N	1	2	3	4	5	6
	$b_r = 1$	110	010	011	001	101	100
$b_\Phi = 0$	$b_r = 0$	111	000	111	000	011	001
	$b_r = -1$	101	100	110	010	011	001
	$b_r = 1$	010	010	011	001	101	100
$b_\Phi = 1$	$b_r = 0$	000	000	111	000	111	000
	$b_r = -1$	001	001	101	100	110	010

Table 3
Comparison of the *V* / *f*, IFOC and DTC control techniques

	V / *f*	IFOC	DTC
Principle	Keep *V* / f constant	Decoupling of stator current components	Optimal selection of the space voltage vector
Controlled size	Amplitude	Amplitude and phase	Amplitude and phase
Dynamic response	Poor / Low	Good	Good
Parameter sensitivity	Average	High	Negligible
In / Out	Regulation of the rotor speed / PWM signals	Regulation of the rotor speed / PWM signals	Voltage and current / Space voltage vector
Sensor speed	Secondary	Necessary	Needless
Complexity and easiness	Simple	Heavy due to the PI controller	Simple
Cost	Cheap	Expensive	Moderate

4. DTC Modeling, Experimental Test Set up and Discussion

4.1. DTC Modeling and Simulation Results

The Matlab/Simulink simulation tool is very helpful to design and implement the global PV-pumping application schematic described in Section 3. It is composed of a PV generator (its modeling is possible using Equation (2)), and a motor-pump controlled by the DTC method. For this purpose, the relations (10)-(13) are used.

The following pictures present the simulation results. It is important to note that the simulations were performed using the same parameters than the experimental ones to highlight the relevance of the proposed PV pumping system.
The voltage waveform, determined at a constant irradiance value (G = 680 W/m^2) and an ambient temperature (T) equal to 27.5 °C (values that can typically be measured in Algeria in July), is shown in Figure 9. At start up, the PV voltage reaches the optimal value at t = 700 ms and oscillates around the MPP.

Regarding the SPIM, torque and flux responses are illustrated in Figure 10, Figure 11, Figure 12, Figure 13, and Figure 14, respectively.
The waveform of the electromagnetic torque oscillates around the load torque value. Even if the motor is troubled by increasing the load torque at t = 10 s from 0.7 N.m to 1 N.m, the electromagnetic torque follows the load torque and still oscillates around this value, validating the expected behavior.
The stator flux is maintained constant, at the set value of 0.6 Wb.

Figure 14 shows that the rotor speed reaches the value of 175 rad/s at the steady state, and decreases at t = 10 s when the torque increases due to the absence of regulation speed loop.

The flow rate is proportional to the rotor speed as shown in Figure 15. According to a value of 180 V of the PV voltage, the flow rate manages to reach the value of 19 l/min.

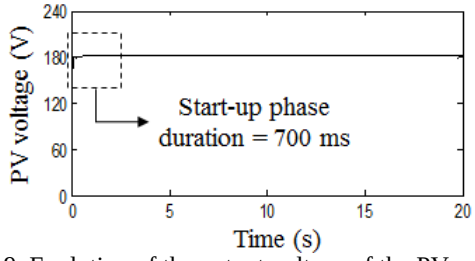


Fig. 9. Evolution of the output voltage of the PV array.

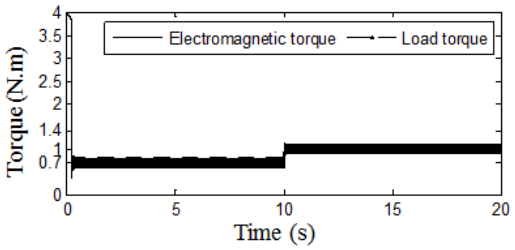


Fig. 10. Electromagnetic torque waveform.

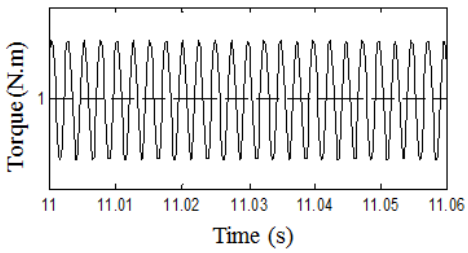


Fig. 11. Zoom on the electromagnetic torque waveform.

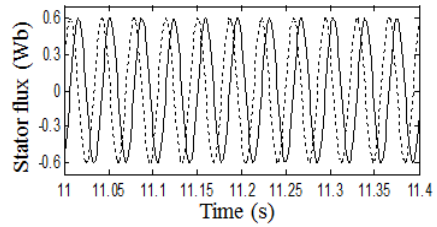


Fig. 12. Zoom on the stator flux waveform.

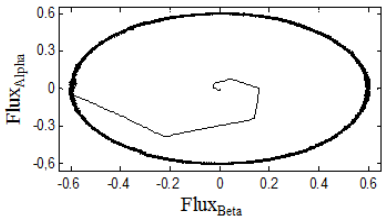


Fig. 13. Zoom on the stator flux waveform.

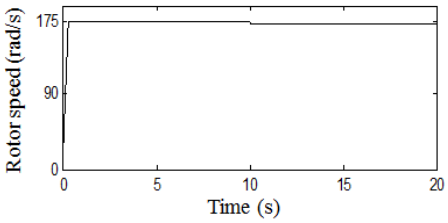


Fig. 14. Zoom on the stator flux waveform.

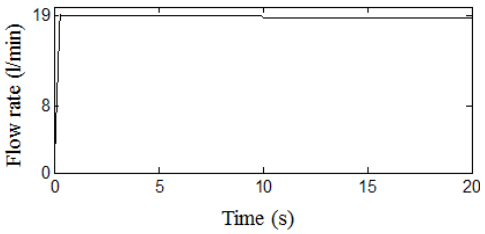


Fig. 15. Flow rate waveform.

4.2. Experimental Tests Procedure, Results and Discussion

The experimental test bench was performed in the LTII laboratory of the University of Bejaia (Algeria) (see Figure 16).

The test bench is composed of a PV generator, a tank of water, a computer to manage the control techniques, a three-phase inverter, a motor-pump system, and a dSPACE1104 card using the TMS320F240 DSP. This card acts as an interface between the Matlab Real-Time Work-shop and the equipment. The current and voltage measurements are insured by current and voltage sensors.

The results come to support the proposed system and are obtained from the Digital Analog Converter of the dSPACE1104 card.

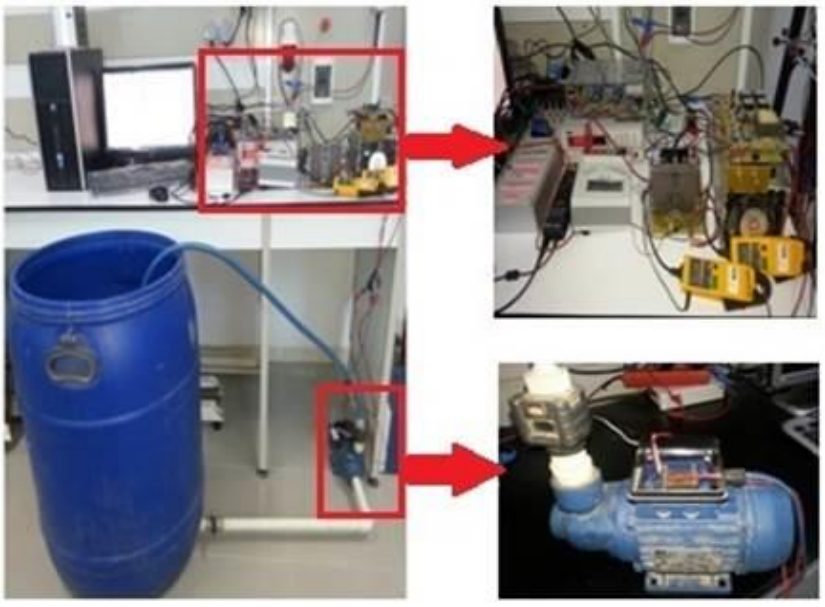


Fig. 16. Experimental test bench of the PV-pumping system.

Figure 17 shows the PV voltage delivered at solar irradiance and ambient temperature equal to 680 W/m^2 and 27.5 °C, respectively. The presence of the ripple is due to the use of P&O MPPT technique. This phenomenon is well described in literature.

As can be seen in Figure 18 and Figure 19, it is important to note that the experimental waveform of the electro-magnetic torque is similar as the simulated signal [32].

As can be seen in Figure 20 and Figure 21, the waveform of the stator flux is sinusoidal with amplitude equal to 0.60 Wb.

Figure 22 shows that the stator flux of the machine has a sinusoidal waveform. This experimental and theoretical signals are the same.

All these experimental results demonstrate the robustness of the DTC control method. As a consequence, the relevance of this kind of application is proven.

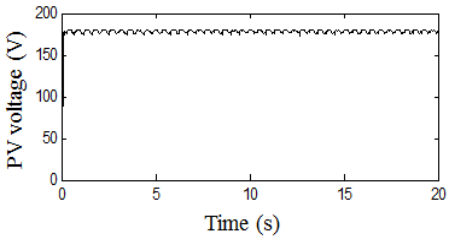


Fig. 17. Flow rate waveform.

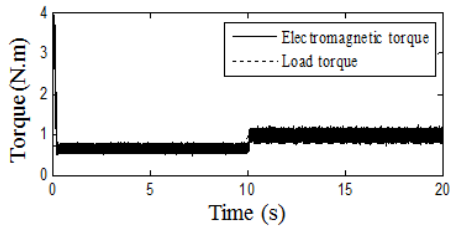


Fig. 18. Flow rate waveform.

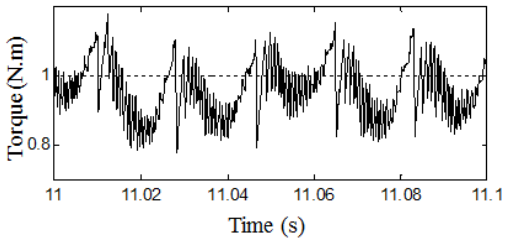


Fig. 19. Flow rate waveform.

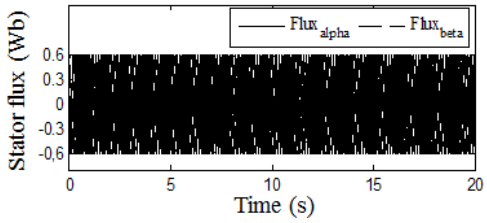


Fig. 20. Flow rate waveform.

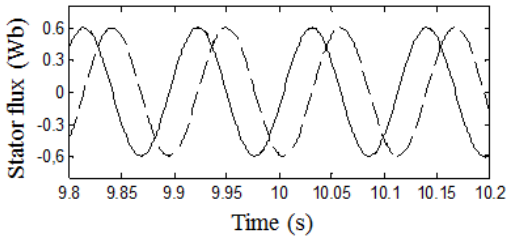


Fig. 21. Zoom on the stator flux waveform in time domain.

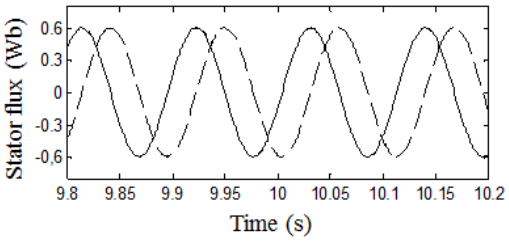


Fig. 22. Stator flux circular trajectory.

5. Conclusions

The aim of this paper is to design and implement a low-cost photovoltaic pumping system that uses a single phase induction motor controlled by the DTC technique. A model of this PV system, based on the Matlab-Simulink simulation tool, has been proposed and validated through-out experimental test results. It is important to note that the method has been validated for a small AC machine, but it may be applied for a huge one.

Despite the fact that ripples are present in the torque waveform, the robustness of the model is verified both in modeling and experimental setup, which allows the ma-chine to be invulnerable to mechanical disturbances.

This PV voltage based on the P&O MPPT technique generates enough power to run the pumping water station un-der the most low-light conditions. The use of the single phase induction motor offers a rugged and cost-effectiveness solution. The whole PV system could be very helpful in rural areas that which are not connected to the national grid.

References

1. X. Liang and O. Ilochonwu, "Induction motor starting in practical applications," IEEE Trans. Industry Applications, vol. 47, no. 1, pp. 271-280, 2011.
2. S. Li, X. Liang, and W. Xu, "Modeling DC motor drive systems in power system dynamic studies," IEEE Trans. Industry Applications, vol. 51, no. 1, pp. 658-668, 2015.
3. ON Semiconductor Technical Note (TND6041/D), DC Motor Driver Fundamentals, Semiconductor Components Industries, LLC, 2014, pp. 1 – 9.
4. M. Z. Youssef, "Design and performance of cost-effective BLDC drive for water pump application," IEEE Trans. Industrial Electronics, vol. 62, no. 5, pp. 3277-3284, 2005.
5. C. L. Su, W. L. Chung, and K. T. Yu, "An energy-savings evaluation method for variable-frequency-drive application on ship central cooling system," IEEE Trans. Industry Application, vol. 50 no. 2, pp. 1286-1294, 2014.
6. C. M. F. S. Reza, Md. D. Islam, and S. Mekhilef, "A review of reliable and energy efficient direct torque controlled induction motor drive," Renewable and Sustainable Energy Re-views, vol. 37, pp. 919-932, 2014.
7. H. Sira-Ramirez, F. Gongalez-Montanez, J. A. Cortes-Romero, and A. Luviano-Juarez, "A robust linear field-oriented voltage control for induction motor: Experimental results," IEEE Trans. Industrial Electronics, vol. 60, no. 8, pp. 3025-3033, 2013.

8. P. K. Beher, M. K. Baher, and A.K. Sahho, "Comparative analysis of scalar & vector control of induction motor through modeling & simulation," International Journal of Innovative Research in Electrical, Electronics, Instrumentation and Control Engineering, vol. 2, no. 4, pp. 1340-1344, 2014.
9. D. H. Jang, "Problems incurred in a vector-controlled single-phase induction motor, and a proposal for a vector-controlled two-phases induction motor," IEEE Trans. Power Electronics, vol. 28, no. 1, pp. 526-536, 2013.
10. C. Mademlis, I. Kioskeridis, and T. Theodoulidis, "Optimiza-tion of single-phase induction motors—part I: maximum energy efficiency control," IEEE Trans. Energy Conversion, vol. 22, no. 1, pp. 187 – 195, 2005.
11. D. Rekioua, S. Bensmail, and N. Bettar, "Development of hybrid photovoltaic-fuel cell system for stand-alone application," International Journal of Hydrogen Energy. Vol. 39, no. 3 pp. 1604-1611, 2014.
12. Z. Mokrani, D. Rekioua and T. Rekioua, "Modeling, control and power management of hybrid photovoltaic fuel cell with battery bank supplying electric vehicle," International Journal of Hydrogen Energy, vol. 39, no. 27, pp. 15178-15187, 2014.
13. Y. Mahmoud, W. Xiao, and H. H. Zeineldin, "A simple approach to modeling and simulation of photovoltaic modules," IEEE Trans. Sustainable Energy on, vol. 3, no. 1, pp. 185-186, 2012.
14. J. J. Soon and K. S. Low, "Photovoltaic model identification using particle swarm optimization with inverse barrier constraint," IEEE Trans Power. Electronics, vol. 27, no. 9, pp. 3975-3983, Sept 2012.
15. M. A. Vitorino, M. B. R. Correa, C. B. Jacobina, and A. M. N. Lima, "An effective induction motor control for photovoltaic pumping," IEEE Trans. Industrial Electronics, vol. 58, no. 4, pp. 1162-1170, 2011.
16. S. Abouda, F. Nollet, A. Chaari, N. Essoumbouli, and Y. Koubaa, "Direct torque control-DTC of induction motor used for piloting a centrifugal pump supplied by a photovoltaic generator," International Journal of Electrical, Computer, Electronics and Communication Engineering, vol. 7, no. 8, pp. 619-624, 2013.
17. I. M. Chergui, and M. Bourahla, "Application of the DTC control in the photovoltaic pumping system," Energy Conversion and Management, vol. 65, pp. 655-662, 2013.
18. M. B. R. Correa, C. B. Jacobina, A. M. N. Lima, and E. R. C. Silva, "Rotor-flux-oriented control of single phase induction motor drive," IEEE Trans. Industrial Electronic, vol. 47, no. 4, pp. 832-841, 2000.
19. G. R. Astorga, J. D. S. Torres, J. C. and A. G. Loukianov, "High-order sliding mode block control of single-phase induction motor," IEEE Trans. Control Systems Technology, vol. 22, no. 5, pp. 1828-1836, 2014.
20. S. Ziaeinejad, Y. Sangsefidi, H. P. Nabi, and A. Shoulaie, "Direct torque control of two-phase induction and synchro-nous motors," IEEE Trans. Power Electronics, vol. 28, no. 8, pp. 4041-4050, 2013.
21. M. Jemli, H. Ben Azza, M. Boussak, and M. Gossa, "Sensorless indirect stator orientation speed control for single-phase induction motor drive," IEEE Trans. Power Electronics, vol. 24, no. 6, pp. 1618-1627, 2009.
22. T. Ouchbel, S. Zouggar, M.L. Elhafyani, M. Seddik, M. Oukili, A. Aziz, and F.Z. Kadda, "Power maximization of an asynchronous wind turbine with a variable speed feeding a centrifugal pump," Energy Conversion and Management, vol. 78, pp. 976-984, 2014.
23. D. Fiaschi, R. Graniglia, and G. Manfrida, "Improving the effectiveness of solar pumping systems by using modular centrifugal pumps with variable rotational speed," Solar Energy, vol. 79, no. 3 pp. 234-244, 2005.
24. T. H. Santos, A. Goedtel and S. A. O. Silva, "Scalar control of induction motor using a neural sensorless," Electrical Power System Research, vol. 108, pp. 322-330.
25. L. Bascetta, G. Maghani, P. Rocco, and A. M. Zanchettin, "Performance limitation in field-oriented control for asynchronous machines with low resolution position sensing," IEEE Trans. Control Systems Technology, vol. 18, no. 3, pp. 559- 573, 2010.
26. I. Takahashi, and T. Noguchi, "A new quick-response and high-efficiency control strategy of an induction motor," IEEE Trans. Industry Applications, vol. IA-22, no. 5, pp. 820-827, 1986.
27. G. S. Buja, and M. P. Kadmierkowski, "Direct torque control of PWM inverter-fed AC motor-a survey," IEEE Trans. Industrial Electronics, vol. 51, no. 4, pp. 744-757, 2004.
28. D. Casadei, F. Profumo, G. Serra, and A. Tani, "FOC and DTC: two viable schemes for induction motors torque con-trol," IEEE Trans. Power Electronics, vol. 17, no. 5, pp. 779-787, 2002.
29. G. S. Buja, and M. P. Kadmierkowski, "Direct torque control of PWM inverter-fed AC motor-a survey," IEEE Trans. Industrial Electronics, vol. 51, no. 4, pp. 744-757, 2004.
30. M. N. Uddin, and M. Hafeez, " FLC-based DTC scheme to improve the dynamic performance of an IM drive," IEEE Trans. Industry Application, vol. 48, no. 2, 2012.
31. B. Metidji, N. Taib, L. Baghli, T. Rekioua, and S. Bacha, "Low-cost direct torque control algorithm for induction motor without AC phase current sensors," IEEE Trans. Power Electronics, Vol. 24, no. 9, pp. 4132-4139, 2012.
32. S. Aissou, S. Jacques, Z. Mokrani, D. Rekioua, T. Rekioua, and A. Ouahabi, "Relevance of the P & O MPPT Technique in an Original PV-Powered Water Pumping Application," Journal of Energy and Power Engineering, Vol. 9, no. 11, pp. 1008-1018, 2015.